An Assessment of CFD Effectiveness for Vortex Flow Simulation to Meet Preliminary Design Needs

P. Raj
Lockheed Martin Aeronautics Company
D/73-07, Z/0685
76 South Cobb Drive
Marietta, GA 30063-0685, USA

D.B. Finley
Lockheed Martin Aeronautics Company
Mail Zone 2275
P.O. Box 748
Fort Worth, TX 76101-0748, USA

F. Ghaffari
NASA-Langley Research Center
Mail Stop 286
Hampton, VA 23681-2199, USA

1.0 Introduction

The low-speed flight and transonic maneuvering characteristics of combat air vehicles designed for efficient supersonic flight are significantly affected by the presence of free vortices. At moderate-to-high angles of attack, the flow invariably separates from the leading edges of the swept slender wings, as well as from the forebodies of the air vehicles, and rolls up to form free vortices (see Figure 1).

The design of military vehicles is heavily driven by the need to simultaneously improve performance *and* affordability.[1] In order to meet this need, increasing emphasis is being placed on using Modeling & Simulation environments employing the Integrated Product & Process Development (IPPD) concept. The primary focus is on *expeditiously* providing design teams with high-fidelity data needed to make more informed decisions in the preliminary design stage.

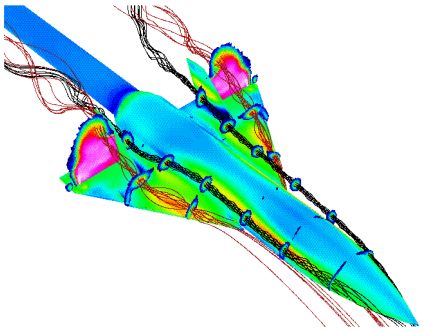

Figure 1. Flow separation from forebody chine and wing leading-edge and roll up to form free vortices

Extensive aerodynamic data are needed to support combat air vehicle design. Force and moment data are used to evaluate performance and handling qualities; surface pressures provide inputs for structural design; and flow-field data facilitate system integration. Continuing advances in computational fluid dynamics (CFD) provide an attractive means of generating the desired data in a manner that is responsive to the needs of the preliminary design efforts. The responsiveness is readily characterized as timely delivery of quality data at low cost.

Lockheed Martin (LM) and National Aeronautics & Space Administration-Langley Research Center (NASA-LaRC) conducted several joint as well as separate studies[2-9] in the 1990s. The studies were aimed at assessing the effectiveness of the state-of-the-art CFD methods (solving Euler and Navier-Stokes equations) in producing aerodynamic data for preliminary design of combat air vehicles. The principal focus was on flight conditions where the flow is dominated by free vortices. In the present context, effectiveness is defined as the ability to meet the desires and expectations of the design teams. It is expressed as a product of two factors: *quality* and *acceptance*. Accuracy and credibility of results are the *quality* factors, and timeliness and affordability of the process of generating those results are the *acceptance* factors.

CFD methods for vortex-flow simulation can be broadly categorized into lower-order methods (based on potential-flow equations), inviscid Euler methods, and viscous Navier-Stokes (N-S) methods. The lower-order methods rate high in acceptance factors because of rapid turnaround and low levels of labor and computer resources. But their rating for quality factors is quite low because their simplified physics model does not allow capturing nonlinear aerodynamic effects such as transonic compressibility. By virtue of the proper model of flow physics, viscous N-S methods alleviate the deficiencies of the lower-order methods.

Paper presented at the RTO AVT Symposium on "Advanced Flow Management: Part A – Vortex Flows and High Angle of Attack for Military Vehicles", held in Loen, Norway, 7-11 May 2001, and published in RTO-MP-069(I).

Report Documentation Page

Form Approved
OMB No. 0704-0188

1. REPORT DATE	2. REPORT TYPE	3. DATES COVERED
00 MAR 2003	**N/A**	**-**

4. TITLE AND SUBTITLE	5a. CONTRACT NUMBER
An Assessment of CFD Effectiveness for Voltex Flow Simulation to Meet Preliminary Design Needs	5b. GRANT NUMBER
	5c. PROGRAM ELEMENT NUMBER
6. AUTHOR(S)	5d. PROJECT NUMBER
	5e. TASK NUMBER
	5f. WORK UNIT NUMBER
7. PERFORMING ORGANIZATION NAME(S) AND ADDRESS(ES) **NATO Research and Technology Organisation BP 25, 7 Rue Ancelle, F-92201 Neuilly-Sue-Seine Cedex, France**	8. PERFORMING ORGANIZATION REPORT NUMBER
9. SPONSORING/MONITORING AGENCY NAME(S) AND ADDRESS(ES)	10. SPONSOR/MONITOR'S ACRONYM(S)
	11. SPONSOR/MONITOR'S REPORT NUMBER(S)

12. DISTRIBUTION/AVAILABILITY STATEMENT
Approved for public release, distribution unlimited

13. SUPPLEMENTARY NOTES
Also see: ADM001490, Presented at RTO Applied Vehicle Technology Panel (AVT) Symposium held inLeon, Norway on 7-11 May 2001, The original document contains color images.

14. ABSTRACT

15. SUBJECT TERMS

16. SECURITY CLASSIFICATION OF:			17. LIMITATION OF ABSTRACT	18. NUMBER OF PAGES	19a. NAME OF RESPONSIBLE PERSON
a. REPORT	b. ABSTRACT	c. THIS PAGE			
unclassified	**unclassified**	**unclassified**	**UU**	**14**	

However, a significant increase in required resources severely hampers their effectiveness for preliminary design applications. As illustrated in Figure 2, inviscid Euler methods offer an attractive alternative to the viscous N-S methods.

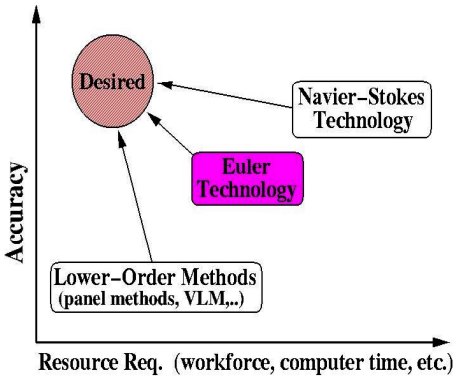

Figure 2. Relative levels of effectiveness of CFD methods for vortex flow simulation

Extensive applications of structured-grid Euler methods throughout the 1980s clearly demonstrated their ability of modeling vortex flows.[10,11] But their effectiveness for preliminary design applications continues to be severely hampered by long turnaround times (2-4 weeks) and large number of labor hours (200-300 hours) associated with their use. The unstructured-grid methods that evolved during the late '80s and early '90s showed considerable promise in alleviating precisely these drawbacks of the structured-grid methods. Projections for unstructured-grid methods ranged from 1-3 days of turnaround times and 25-50 labor hours by the end of the 1990s. This development was the prime motivator behind the present study by NASA and industry aimed at evaluating the effectiveness of unstructured-grid methods in predicting vortex flows and associated aerodynamic characteristics of combat air vehicles in a preliminary design environment. The basic approach is outlined in Section 2. Typical results are presented in Section 3 that illustrate effectiveness of Euler CFD methods in estimating configuration effects, compressibility effects and control effects. A few concluding remarks in Section 4 complete this paper.

2.0 Approach

The approach to assessing the effectiveness of unstructured-grid Euler methods involved analyzing representative combat air vehicle configurations using state-of-the-art methods. Turnaround time, labor and computer resources were recorded to evaluate the ability of these methods to provide timely and affordable solutions. Prediction accuracy was assessed by correlating computed solutions with measured data.

Prior to focusing the investigation on unstructured-grid Euler methods, a feasibility study was conducted by Ghaffari[2] of NASA-LaRC. It involved using the structured-grid CFL3D[12] code and the unstructured-grid USM3D[13] code on a relatively simple configuration. The objective was to carefully assess the implications of neglecting viscous effects on vortical flow predictions. Key findings are summarized in Section 3.1. This study was followed by a more extensive investigation sponsored by NASA-LaRC and conducted with industry participation. It involved several different Euler methods and relevant slender, sharp-edged configurations. The selected CFD methods included the unstructured-grid USM3D code,[13] unstructured Cartesian-grid SPLITFLOW code,[14] multi-block structured-grid TEAM code,[15] multi-block overset structured-grid OVERFLOW code,[16] and multi-block structured/unstructured NASTD code.[17] These methods were used to analyze (a) the NASA-LaRC Modular Transonic Vortex Interaction (MTVI) configuration––a generic fighter research model, (b) the Lockheed Martin Innovative Control Effectors (ICE) model, and (c) the Boeing Aero Configuration/Weapons Fighter Technology (ACWFT) model. The results from these analyses are reported in References 2-9, 18 and 19.

This paper includes results of only two configurations, MTVI and ICE, and two codes, USM3D and SPLITFLOW. Key geometrical features of the configurations are described in Section 2.1, and the flow conditions used for analyses are presented in Section 2.2.

2.1 MTVI and ICE Configurations

The MTVI configuration has a cropped-delta wing mounted on a fuselage that has a chine forebody with an included angle of either 100^o or 30^o. The wing has 60^o leading-edge sweep, 1.8 aspect ratio, and a segmented leading-edge flap. In addition, the model is designed to accommodate either a centerline tail (CT) on the fuselage or twin tails (TT) on the wing as shown in Figure 3(a). This configuration and its variations are defined analytically through series of algebraic circular-arc and cubic relationships. Representative sting geometry was included in the numerical model to represent the wind-tunnel model support. All components including forebody chine, wing planform edges, vertical tails, and leading-edge flaps have sharp edges.

An extensive experimental database (led by Dr. Robert M. Hall of LaRC) has been developed for the various MTVI variants across a wide range of flow conditions to assist in the study of complex vortical flows generated by this class of vehicles at moderate to high angles of attack. Such complex flows include vortex-vortex interaction, vortex breakdown, vortex-tail interactions, etc. In addition to forces and moments, the experimental data consists of surface pressures measured at six fuselage stations (FS), three on the forebody chine and three on the wing-fuselage portion, shown in Figure 3(a). This database provides a unique set of results for calibrating CFD prediction capabilities for this class of vehicles.

A composite of two ICE configurations is shown in Figure 3(b), one with straight trailing edge (bottom half) and the other with serrated edge (top half). Both configurations have blended wing, fuselage and canopy, with a substantial amount of camber near the leading edge. The wing, representative of combat air vehicles, is 4% thick with 65^{o} leading-edge sweep and NACA 64-A airfoil section. Trailing-edge control effectors include elevons and spoilers. The wind-tunnel models have no pressure taps; only force and moment data are available for comparisons.

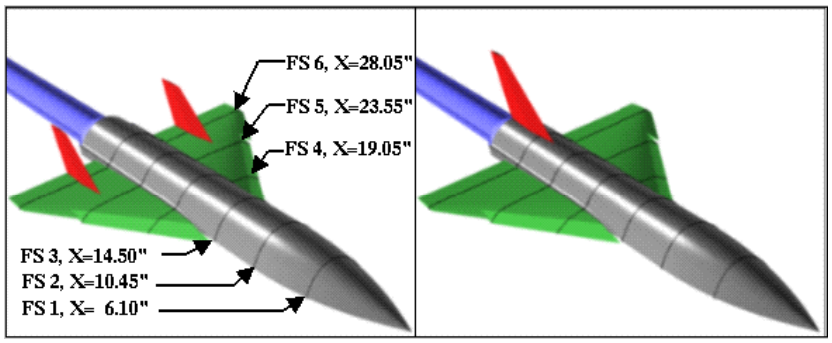

Figure 3(a). MTVI Twin-Tail (left) and Centerline-Tail (right) configurations

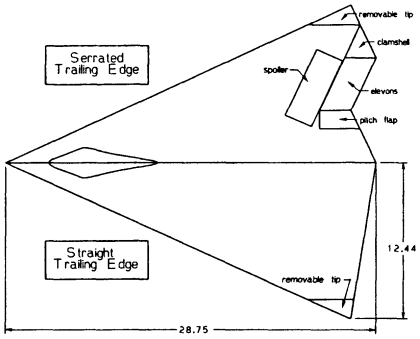

Figure 3(b). ICE Configuration

2.2 Analysis Conditions

Both MTVI and ICE configurations were analyzed for a wide range of angles of attack and several yaw angles at subsonic and transonic Mach numbers. As an example, the run matrix for the MTVI configurations is shown in Table 1 for a total of 42 runs. A similar matrix for the ICE configuration, with and without control devices, included 50 runs. It covered both subsonic and transonic Mach numbers, and a range of angles of attack up to 30 degrees and of yaw angles up to 10 degrees.[8,9]

Table 1. Run Matrix for MTVI Analysis

Model	Mach No. (M)	Angle of Attack (α)	Yaw Angle (β)	No. of Runs
MTVI TT	0.4, 0.85	10, 12.5, 15, 17.5, 20, 25, 30 25	0 2,4,7	14 6
MTVI CT	0.4, 0.85	10, 15, 20, 25, 30 15, 25	0 2,4,7	10 12

Computed forces, moments, surface pressures and flow-field data were compared with available experimental data to assess the effectiveness of the CFD methods. Representative results are presented in the next section.

3.0 Results and Discussion

In this section, representative results are presented for the MTVI and ICE configurations. Key findings of the feasibility study using the MTVI isolated fuselage model are discussed in Section 3.1. These findings, combined with those obtained from other studies undertaken early on to assess the impact of neglecting viscous effects,[3,18] provided the necessary justification for performing a more extensive evaluation of inviscid unstructured-grid Euler methods. An assessment of the effectiveness of two Euler methods, USM3D and SPLITFLOW, in predicting configuration effects (tail placement and chine shape) is given in Section 3.2, compressibility effects in Section 3.3, and control effects in Section 3.4.

3.1 Feasibility Study

Viscous and inviscid analyses of the MTVI isolated fuselage model were performed using the CFL3D code,[12] and inviscid analysis using the USM3D code.[13] Figure 4 shows the normalized total-pressure contours ($p_{o,l}$ /p_o) at three fuselage stations from CFL3D (starboard) and USM3D (portside) computations for α = 19.8°, M = 0.4. The turbulent viscous results for R_{ft} = 2.4x10^6 are based on the Baldwin-Lomax turbulence model with Degani-Schiff modification. All results are plotted over the same range {($p_{o,l}$ /p_o)$_{min}$ = 0.86, ($p_{o,l}$ /p_o)$_{max}$ = 1.0} and levels {($p_{o,l}$ /p_o)$_{increment}$ = 0.0175}. The CFL3D and USM3D inviscid results qualitatively show similarities in the size and trajectory of the primary vortex-flow structure. The viscous CFL3D results show a somewhat larger primary vortex, along with a secondary vortex and a thin boundary-layer region near the surface. Note that the viscous primary-vortex core appears to be more diffused, due to viscous damping, than the inviscid results where the contour-level structures are more compact and clustered.

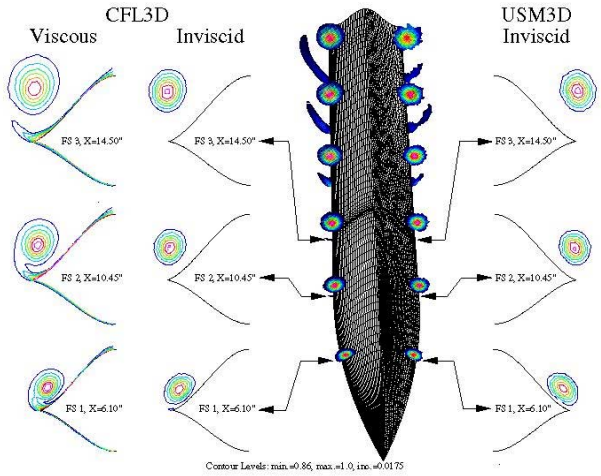

Figure 4. Normalized total-pressure predictions based on structured and unstructured grid methodologies, α = 19.8°, M = 0.4, R_{ft} = 2.4x10^6

In Figure 5, the computed surface pressure coefficients (C_p) obtained from the structured- and unstructured-grid methods are correlated with the experimental data. Note that the data are shown for both the port and the starboard sides of the model to assess any flow asymmetry. Results are shown at the same stations as those in Figure 4. The inviscid results obtained from the structured and unstructured grid methods are in excellent agreement with each other. The viscous results show reasonable agreement with the measured surface pressure coefficients, but the inviscid predictions indicate generally a higher primary-vortex suction peak, i.e., more negative C_p, that is located slightly outboard. Similar computational results and correlation with experimental data were observed for M = 0.4, α = 29.8°, R_{ft} = 2.3x10^6.

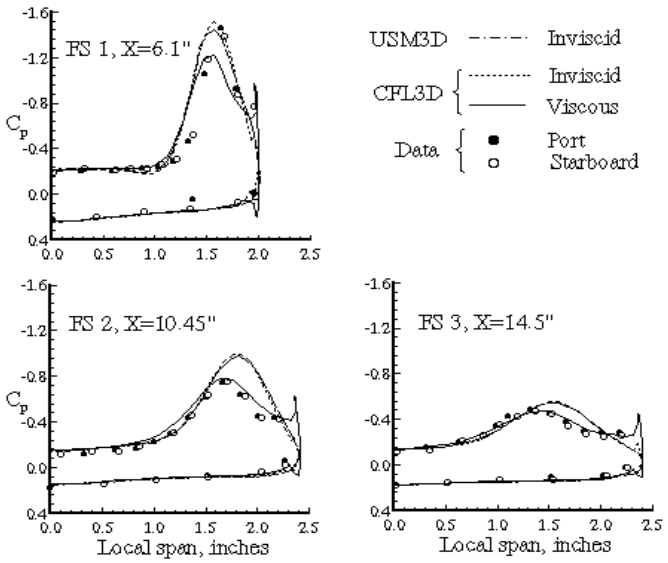

Figure 5. Computed and measured surface pressures, α = 19.8°, M = 0.4, R_{ft} = 2.4x10^6

The computed longitudinal aerodynamic characteristics are correlated with experimental data in Figure 6. The forces and moments predicted by the thin-layer Navier-Stokes method, CFL3D, compare very well with the experimental data. It is also interesting to note that the inviscid Euler predictions correlate reasonably well with the measurements, despite the differences with viscous solutions in vortex flow structure and surface pressure coefficients as shown in Figures 4 and 5. This effect, which manifests itself only on the overall aerodynamic data, is attributed to the integration process over local flow properties (i.e., surface pressures) to numerically determine the global aerodynamic characteristics. The integration process inherently does not maintain the variable local changes such as the difference between the inviscid and viscous surface pressure distributions.

This NASA-LaRC feasibility study, combined with others[10,11] performed by numerous investigators using structured-grid Euler methods during the 1980s, demonstrated that for sharp-edged vehicles the

inviscid Euler analysis is a viable approach for computing aerodynamic data with sufficient accuracy for preliminary design efforts. It cannot be overemphasized that Euler analyses and results require *careful interpretation* due to the inherent limitations of the inviscid model of flow physics.

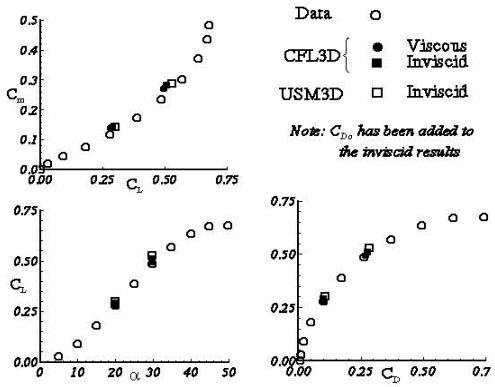

Figure 6. Computed and measured longitudinal aerodynamic characteristics, M = 0.4, R_{ft} = 2x10^6

3.2 Configuration Effects

In this section, results for MTVI analyses are presented to illustrate the effectiveness of Euler methods in simulating tail-placement and forebody chine-shape effects.

Tail Placement Effect—Representative on- and off-surface flow features obtained using USM3D on the MTVI CT and TT configurations having forebody chine with included angle (ϕ) of 100^o are shown in Figure 7. The figure shows the computed surface pressures, off-surface total pressure contours at six longitudinal cross-flow planes (that coincide with the stations where surface pressures were measured), and particle traces through the wing and forebody vortex cores. The figure clearly demonstrates the effects of vertical tail arrangement on the configuration surface and off-surface flow fields. A typical MTVI computation, with about 0.8 million tetrahedral cells generated using VGRID,[20] required 200 megawords (MWs) of memory and approximately 5 hours of computing time on a Cray C90.

The computed Euler surface pressure distributions for the MTVI CT and TT configurations are correlated with experimental data at FS 3 (X = 14.5") through FS 6 (X = 28.05") in Figure 8. The effect of different vertical tail arrangements on forebody surface pressures at FS 3 is quite small, both computationally and experimentally. Note the expected trends in the computed surface pressure distribution relative to data, i.e., higher primary vortex suction peak located slightly outboard and no evidence of secondary-vortex loading. The experimental data over the wing sections generally indicate higher suction peak levels for the CT than the TT configuration, and both exhibit pressure distributions consisting of two distinct suction peaks associated with the wing and the forebody chine vortices. The pressure distributions predicted over the wing by the Euler method, however, show some characteristics that are different than experimental data as discussed next.

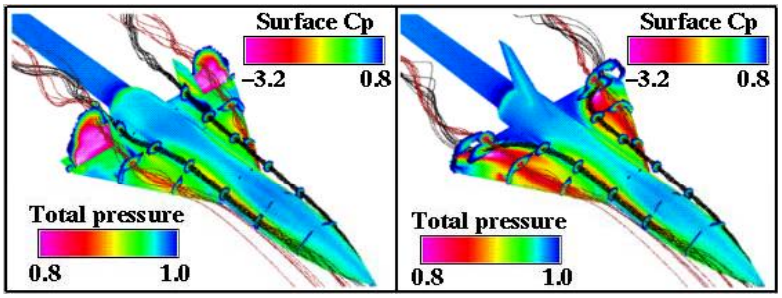

Figure 7. Computed on- and off-surface flow features for MTVI TT and CT models, ϕ = 100^o, δ_{flap} = 30^o, α = 22.5^o, M = 0.4

At FS 4 (X = 19.05") in Figure 8, the computed results generally show the correct pressure trends in suction peaks associated with the wing and chine vortices, though the magnitudes are somewhat off compared to the data. Also, the computed pressure distribution indicate a low pressure region in between the wing and the chine vortex suction peaks (i.e., 2.5 < Y <3.5). This low-pressure region can be attributed to the inboard expansion of the wing primary vortex over the flap hinge-line onto the main wing panel. The effect of this inboard expansion of the wing primary vortex over the flap hinge line and the resulting suction peak is even more pronounced at FS 5 (X = 23.55") for both the TT and the CT models (see Figure 7 for the corresponding computed vortical flow visualization). At FS 6 (X = 28.05"), the computed results for the TT model show a slight overprediction of the wing pressures in the separated flow region outboard of the tail (Y >5), and the predicted suction peak associated with the chine forebody vortex appears to be further outboard than the data indicate. The computed pressures for the CT model clearly show a single suction peak that appears to coincide with a region of the flow (see Figure 7) where the forebody vortex and the wing vortex

coalesce. This coalescing of the two vortices at this station gives rise to such an extreme low-pressure suction peak that is not present in the experimental data.

The computed lift, drag and pitching moment coefficients for the MTVI TT configuration correlate exceptionally well with the experimental data both in terms of magnitude and trends across the examined range of flow conditions, except at the extreme angle of attack of 45^o as shown in Figure 9. The computed results for the MTVI CT configuration, however, compare well with the data only at the low angle of attack of 10^o. The Euler code overpredicts the lift coefficient (C_L) at the higher angle of attack of 22.5^o and underpredicts it at 30^o. This effect could be caused by the complexities of the chine and wing vortex interactions that are very difficult to numerically simulate and obtain good solution convergence. Despite the disagreement in the magnitudes of the predicted and measured lift coefficients at higher angles of attack, the overall trend for vertical tail placement effects is computed correctly by the code. This trend shows that the MTVI CT model produces higher lift, lower drag and an increase in the nose-down pitching moment relative to the MTVI TT model for $\alpha > 10^o$.

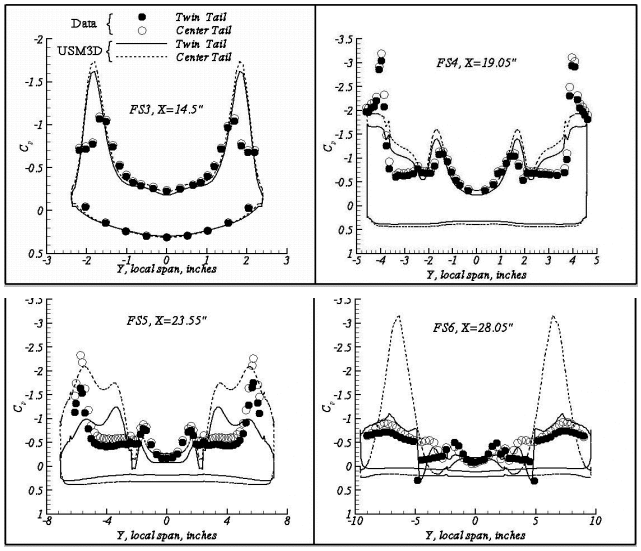

Figure 8. Surface pressure correlation for MTVI TT and CT models, ϕ = 100^o, δ_{flap} = 30^o, α = 22.5^o, M = 0.4

The MTVI configurations were also analyzed by Finley et al[4] for symmetric and asymmetric conditions using the SPLITFLOW code. The SPLITFLOW predictions were similar to those of the USM3D code. Generally, the computed longitudinal coefficients matched well with data; but the lift and nose-down moment predictions from SPLITFLOW were higher than those from USM3D due to grid adaption as discussed later on in Section 3.3. Compared to the longitudinal coefficients, lateral-directional coefficients showed more variation and sensitivity to the absence of viscous effects in predicting vortex placement. For the TT configuration, the SPLITFLOW accurately predicted the lateral-directional data both in terms of trends and magnitudes. However, the nonlinear variations in the data were not well predicted for the CT configuration. For example, the Euler computation did not capture a non-linearity at α = 30^o and β = 3^o. This non-linearity could correspond to a burst vortex condition. Pressure data indicate that the lee-side wing vortex causes a severe reduction in peak values at the last two fuselage stations, while the computation shows significant suction. The integrated forces from the test data indicate that more negative side force is generated on the CT than the TT configuration. The side force for the CT configuration is overpredicted compared to that for TT, but it is consistent with the incremental increase in yawing moment seen for the CT model. Therefore, the Euler code accurately predicts the configuration change effects on stability for this case.

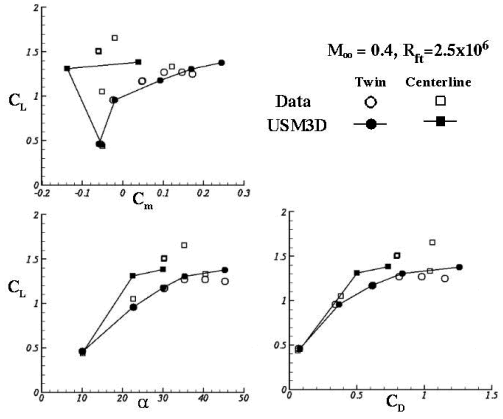

Figure 9. Effects of vertical tail arrangement on MTVI longitudinal aerodynamic characteristics, ϕ = 100^o, δ_{flap} = 30^o

In summary, both CFD methods performed well in predicting the wing pressures for the TT configuration. The low-energy flow region on the outer wing panel outboard of the twin vertical tails is well predicted. The predicted behavior appears analogous to a large-scale separated flow zone. For the centerline tail arrangement the code overpredicts the primary vortex suction peak pressure on the wing. This

corresponds to an overprediction of normal force and nose-down pitching moment. In general, the Euler predictions capture the significant primary-vortex flow features, but miss the secondary separation.

Chine Shape Effects—The computed and measured surface pressure distributions for the MTVI TT configuration with two different forebody chine angles are shown in Figure 10 at two representative fuselage stations. The experimental data on the forebody station (FS 3) indicate that the primary vortex suction peak moves inboard and becomes less negative for the smaller chine angle. This trend is clearly captured by the Euler method. Similar to the results for tail placement discussed above, the general characteristics of the pressure distributions are captured by the Euler computations (i.e., higher suction peak, located slightly outboard, and no evidence of a secondary vortex loading). The experimental data at the most aft wing-body station (FS 6) indicate little sensitivity to different chine angles. Also note the asymmetry in measured wing pressures in the separated flow region outboard of the vertical tail for the 30°-chine model. Though, not shown here, the effect of different chine angle on the overall aerodynamic characteristics were small and the Euler method captured the effects in a reasonable manner.

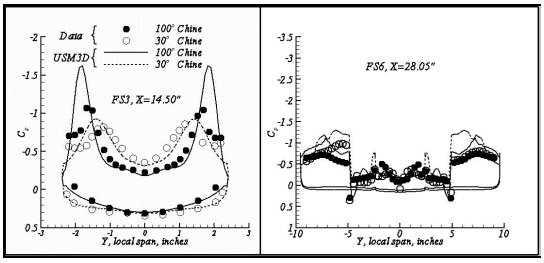

Figure 10. Computed and measured MTVI TT surface pressures, $\delta_{flap} = 30^o$, $\alpha = 22.5^o$, M = 0.4, $R_{ft} = 2.5x10^6$

The SPLITFLOW code also provided good agreement with the force coefficients for the sharper chine, including the nose-up pitching moment break above C_L of 1.0. The model with 30° chine angle has a slight increase in lift, and a nose-up pitching moment, compared to the one with 100° chine angle.[3] The Euler predictions showed the trend of inward movement of the suction peak, but tended to underpredict the peak in suction pressure on the forebody.

3.3 Compressibility Effects

In order to assess the effectiveness of Euler methods for predicting compressibility effects, MTVI CT and TT configurations with 30° chine and 0° flap deflection were analyzed at Mach numbers of 0.4 and 0.85. A large number of symmetric and asymmetric flow conditions were investigated (see Table 1). References 4-6 contain extensive comparisons of computed results with test data. In general, predictions for transonic flow (M = 0.85) matched better with experimental data than those for subsonic flow (M = 0.4). The surface pressures show large over-expansion at subsonic speeds which is much less pronounced at transonic speeds. Only a few sample results for each configuration are included here.

For the USM3D analysis, the grid for the CT model contained over 600K cells, and for the TT model over 800K cells. The SPLITFLOW analysis used about 500K cells for each model. For symmetric cases, both USM3D and SPLITFLOW produced converged solutions in 400 to 600 cycles using the implicit solver. The CPU times averaged 3 hours on Cray C-90, and the required memory ranged from 110 to 120 MWs. The asymmetric cases required 600 to 700 cycles for USM3D and 800 to 1000 for SPLITFLOW. The corresponding CPU times were about 8 hours for USM3D and 14-18 hours for SPLITFLOW, and the memory requirements ranged from 200 to 230 MWs.

MTVI CT Results—For the symmetric flow cases, Figure 11 shows the computed lift and drag coefficients from both codes. At subsonic speeds (M = 0.4) the predictions correlate well with each other and with experimental data for $\alpha < 20^o$ where the vortical flow field is benign. At higher angles of attack, results from both codes differed from each other as

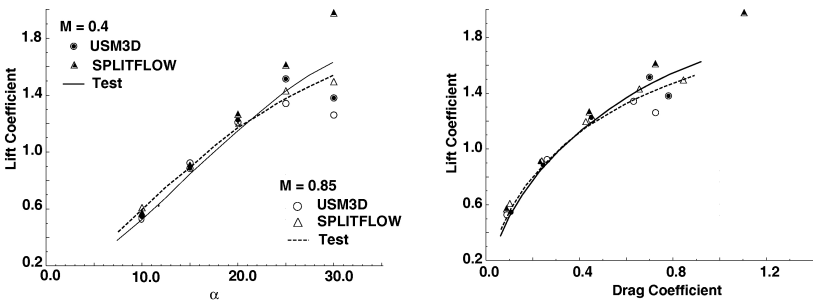

Figure 11. Lift and Drag correlation for MTVI CT configuration

well as from test data. The largest differences were seen for the 30° case. The SPLITFLOW code produced a solution with benign vortex flow and significantly overpredicted lift and drag. The USM3D solution, in contrast, exhibited burst vortex flow and underpredicted lift and drag. The most likely cause of this discrepancy is the use of grid adaption in SPLITFLOW; a fixed grid is used in USM3D. SPLITFLOW clusters cells in the vicinity of the vortex where gradients are large, and thereby keeps numerical dissipation to relatively low levels. Without grid adaption in the USM3D analysis, the vortex core meanders to regions where cells are relatively large with correspondingly higher levels of dissipation. This issue needs to be further investigated to better assess the effectiveness of inviscid Euler analyses in predicting vortex bursting.[7]

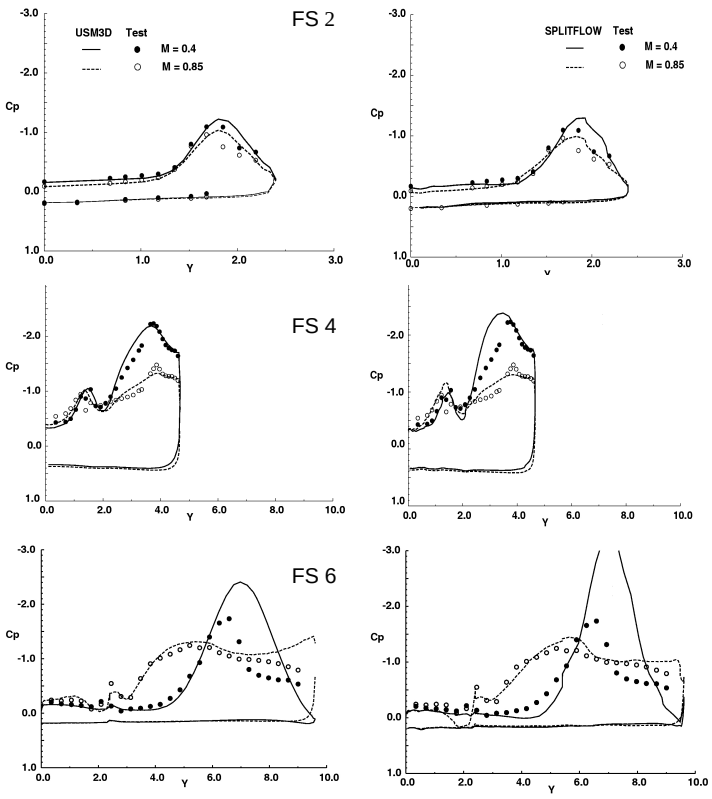

Figure 12. Comparison of USM3D (left) and SPLITFLOW (right) predictions for compressibility effects on MTVI CT configuration, $\alpha = 20^o$, M = 0.4 and 0.85

For the transonic cases (M = 0.85), computed lift and drag coefficients generally correlated well with data for the entire range of angle of attack. It should also be noted that the pitching moment correlation (not included here) showed that both codes predicted the trends but discrepancies with test data increased with increasing α.

Typical results for the $\alpha = 20^o$ case are shown in Figure 12 at three representative stations**.** In general, the computed surface pressures compared well with test data on the forebody station, and in particular, increments due to compressibility were well predicted. For the wing-body stations, computed results matched well with test data but discrepancies increased with increasing distance from the nose. The discrepancies were quite noticeable at the last station, especially for the subsonic case. The surface pressures show large overexpansion at subsonic speed that is much less noticeable at transonic speed.

MTVI TT Results—Figure 13 shows correlation of computed and measured lift and drag coefficients for the symmetric flow cases. For subsonic cases, the computed lift and drag coefficients from both codes correlated well with each other and with experimental data for $\alpha < 20^o$ where the model exhibits benign vortical flow field. At higher angles of attack, results from both codes differed from each other as well as from data. The largest differences were seen for the 30° case. Even though the SPLITFLOW code overpredicted lift and drag, the magnitude of the discrepancy was not as large as that for the CT case (Figure 11). For the transonic cases, M = 0.85, computed lift and drag coefficients showed very good correlation for the entire range of angle of attack. A particularly noteworthy feature was the ability of both codes to

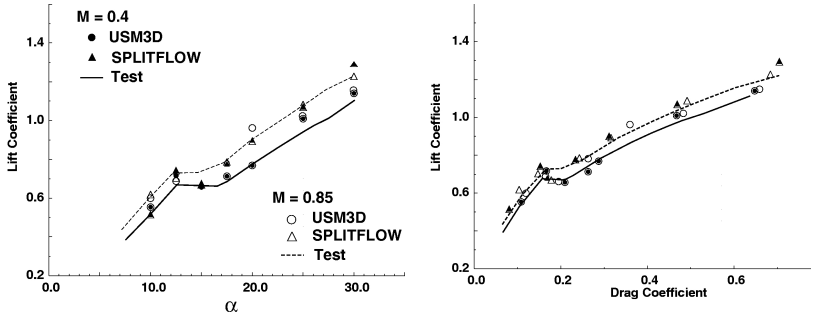

Figure 13. Lift and drag correlation for MTVI TT configuration

accurately capture the break in the lift and drag variation for α between 12.5^o and 17.5^o. This break is due to wing and chine vortex interactions with the twin vertical tails.[5] Also, both codes predict the pitching moment trends (not included here), but discrepancies with test data increased with increasing angle of attack.

The computed surface pressures generally compared well with test data at the forebody station as shown in Figure 14. Much like the CT case, the computed compressibility increments were in good agreement with the measured ones. For the two stations on the wing-body portion shown in Figure 14, computed results matched well with test data. The results confirm that the primary compressibility effects are well captured by the Euler simulations using both USM3D and SPLITFLOW codes. This is especially true for the increments.

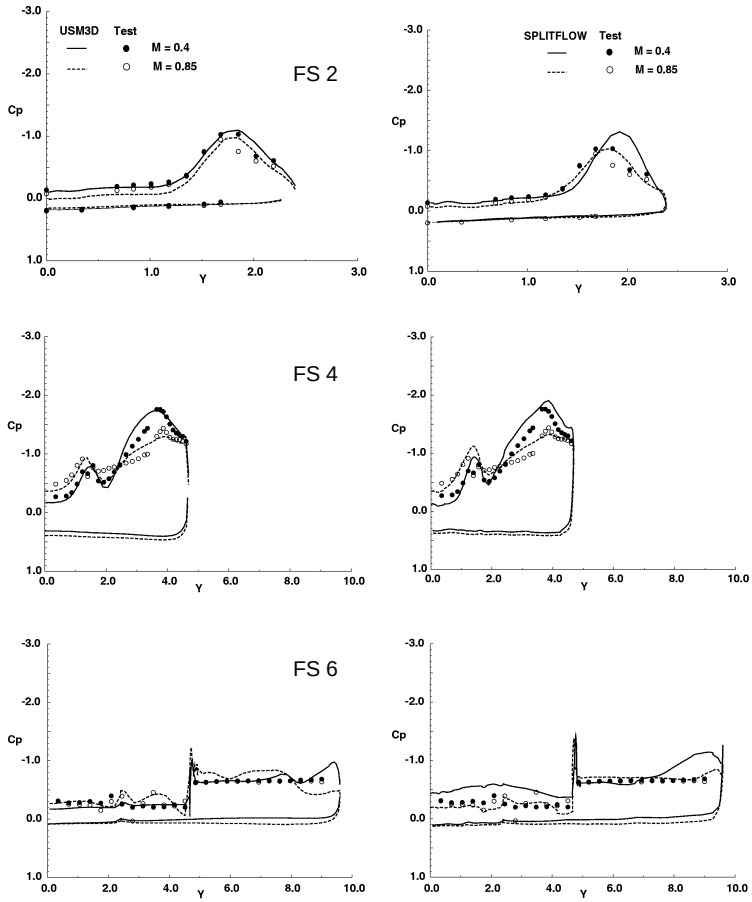

Figure 14. Comparison of USM3D (left) and SPLITFLOW (right) predictions for compressibility effects on MTVI TT configuration, α = 20^o, M = 0.4 and 0.85

3.4 Control Effects

The prediction of control effects highlights the important role of CFD in vehicle design. Frequently, the off-body flow interaction can lead to unanticipated changes in control effectiveness. CFD can provide important screening of potential problems. An extensive study[8] was conducted using the ICE configuration to assess the effectiveness of the SPLITFLOW code in predicting aerodynamic characteristics due to deployment of leading-edge flaps as well as trailing-edge elevons and spoilers. Euler predictions captured the significant changes in flow characteristics and the direction of the force and moment increments. Data from an attached-flow case (elevon) and a large-scale separated flow case (spoiler) are included here.

First, results for the attached flow case for symmetrically deflected trailing-edge elevon on the ICE vehicle are shown in Figure 15. The normal force (C_N), axial force (C_A) and pitching moment (C_m) increments due to deflection match quite well with the measured increments except at 18^o angle of attack, where the code overpredicts the normal force and nose-down moment. On further investigation, it was found that for some angles of attack such as this, the solution had difficulty in converging and the force and moment predictions settled in at levels that did not correlate well with data. At other angles of attack both above and below the troublesome one, the solution proceeded much better in terms of convergence and predictions correlated well with test data.

The CFD code generally predicted the trend in the force and moment data correctly, even more so for cases of massive change in flow structure such as that caused by a spoiler deflection. This is illustrated in the prediction of incremental forces and moments for the 60^o deflected spoiler case shown in Figure 16. Once again predictions for some angles of attack agree well with data while others do not. The side force and lateral-directional coefficients for this asymmetric deflection show good correlation with data trends, except for the highest angle of attack of 25 degrees. It was found that the code would indicate changes in the character of force data, such as removal of a jog in the normal force curve or change in slope of axial force. The large-scale physical change in flow character is also predicted.

Visualization of the off-body flow structure is a significant benefit of the CFD analysis. An example of the flow around the ICE model at $\alpha = 20^o$ with spoiler deflection of 60^o is shown in Figure 17. The complete absence of vortical structure on the starboard side illustrates the code's ability to capture large-scale changes in the flow. The computed results showed a large recirculation zone behind the spoiler on the starboard side, representative of the flow separation observed in tests. Analysis of other conditions indicates the ability of CFD to capture these significant features in the flow field, and predict force and moment increments, which are useful for design. It is again noted that certain combinations of angle of attack, side-slip angle, leading-edge geometry, and control surface deflection posed severe challenges to solution convergence. For some cases, the CFD solution either converged to a result that did not match the measured data or failed to converge properly. This may be a manifestation of the use of pseudo-time-marching in the computations which could not accurately capture the unsteadiness of the actual flow. Hinge-moment analysis at M = 0.9 was applied to the data comparisons for the ICE vehicle. It was found that the inviscid Euler methods predicted the trend in hinge moment vs deflection angle and hinge moment vs model α relatively well for both the spoiler and the elevon.

The grids for these flows had on the order of 400K to 500K cells for the entire flowfield of a full (both left and right side) vehicle. In some cases a pure Cartesian mesh was employed, while in other cases prismatic cells were layered onto the surface triangulation, while Cartesian cells were used for regions away from the body. It was found that this level of grid resolution struck the proper balance between flow field resolution (which includes grid adaption) and run time.

The off-body flow for the ICE vehicle was compared at $\alpha = 24^o$ and $\beta = 10^o$ for two grid resolutions of approximately 400K and 800K cells. Refinement of the mesh to 800K cells did not result in better agreement with test data. The two solutions had the same vortex structure and vorticity pattern (displayed on the aft cutting plane). The larger grid did have 'tighter' vortices and a slightly larger recirculation zone. The amount of grid refinement used, and the refinement criterion, determined the vortex suction

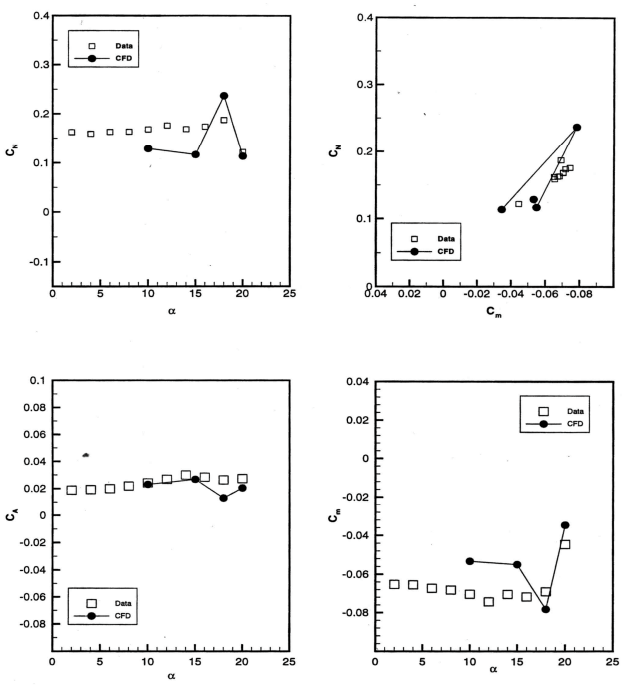

Figure 15. Correlation of incremental forces and moments for ICE configuration with 30^o deflected elevon, M = 0.9

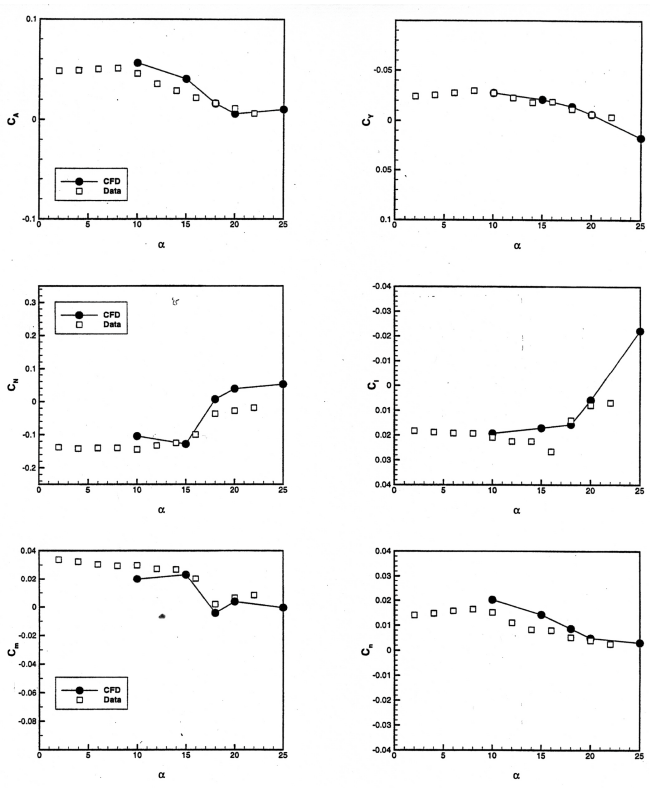

Figure 16. Correlation of incremental forces and moments on ICE configuration for 60^o spoiler deflection, M = 0.9

peak pressure levels. Upon grid refinement, the Euler code further intensified the core rotation and suction peak pressures. This was especially true for the ICE model in sideslip in the vicinity of 24 degrees, where the Euler code results showed significant non-linearity versus the test data.

The repeatability of the predictions was considered good. For example, repeat runs were made at $\alpha = 24^o$ and $\beta = 10^o$ of a complex flow in which the initial condition was brought in from a converged solution at a different angle of attack, then the solution was re-converged at the current condition using either additional adaption or no further adaption. The resulting flow structure and surface data closely matched those obtained from the first analysis. The number of iterations for complex flows was about three times more than that for the benign flow cases. Also, for the complex flow cases, the force and moment predictions required careful analysis. For example, even after a large number of iterations, the computed pitching moment for complex flows fluctuated around a mean value with fluctuation levels of the order of ±0.03 or more. In contrast, for the benign flow cases, the fluctuation levels were much smaller, on the order of ±0.0005. The larger levels of fluctuation indicated a lack of convergence. A much more extensive analysis of the results is required in such cases for proper interpretation.

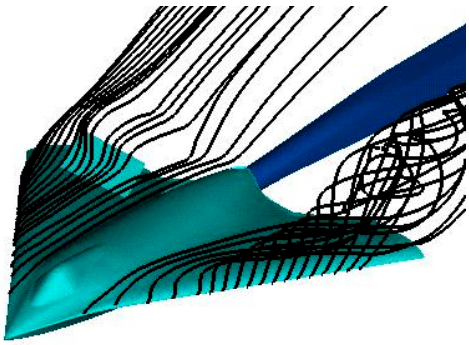

Figure 17. Flow field from SPLITFLOW analysis of ICE configuration with 60^o deflected spoiler, M = 0.9, $\alpha = 20^o$

4.0 Concluding Remarks

Based on the results of the present study, it may be readily concluded that unstructured-grid Euler methods are quite effective in predicting configuration effects, compressibility effects and control effects to support preliminary design of combat vehicles with sharp, swept leading edges. For configuration trade studies in early design stages, Euler methods are efficient given the substantial improvement in turnaround time and cost over viscous Navier-Stokes analysis by a factor of 3 to 5.

In the present study, computed surface pressure predictions were found to be generally in good agreement with test data in attached flow regions, and the primary vortex flow characteristics were well captured. However, the Euler methods missed secondary vortex formation and the primary vortex placement. The magnitude of suction peaks associated with primary vortex structures was overpredicted by the Euler methods compared to measured data, and its location was slightly outboard. Grid adaption to vortex gradients proved very useful in improving the capture of primary vortex features, but in some cases resulted in overprediction of vortex peak suction. In a few cases where the test data indicated unsteady flow, the SPLITFLOW code with grid adaption did not fully converge and produced flow features that were different from those observed in experiments. Clearly, Euler methods are not expected to correctly model certain features of vortex flows that are dominated by viscous effects. Therefore, user expertise in closely examining the solution process and carefully interpreting the results is critical.

Euler methods generally provided reliable trends for integrated forces and moments, which was one of the assessment criteria of the present investigation. However, reliable predictions of force and moment data—in spite of discrepancies in the associated surface pressure distributions—indicate that integrated data alone may not be a true measure of the prediction accuracy. Also, for maximum effectiveness in a preliminary design environment, the accuracy of a simulation must be tempered with the turnaround time and cost factors. Efforts should continue so that Euler and Navier-Stokes methods rapidly become fully effective tools for supporting preliminary design needs.

References

1. Raj, P., “Aircraft Design in the 21st Century: Implications for Design Methods (Invited Paper),” AIAA 98-2895, June 1998.
2. Ghaffari, F., “On the Vortical–Flow Prediction Capability of an Unstructured-Grid Euler Solver,” AIAA 94-0163, January 1994.

3. Finley, D.B., “Euler Technology Assessment Program for Preliminary Aircraft Design Employing SPLITFLOW Code with Cartesian Unstructured Grid Method,” NASA CR 4649, March 1995.
4. Finley, D.B. and Karman, Jr., S.L., “Euler Technology Assessment for Preliminary Aircraft Design—Compressibility Predictions by Employing the Cartesian Unstructured Grid SPLITFLOW Code,” NASA Contractor Report 4710, March 1996.
5. Kinard, T.A. and Raj, P., “Euler Technology Assessment for Preliminary Aircraft Design—Compressibility Predictions by Employing the Unstructured Grid USM3D Code,” NASA Contractor Report 4711, March 1996.
6. Kinard, T.A., Finley, D.B., and Karman, Jr., S.L., “Prediction of Compressibility Effects Using Unstructured Euler Analysis on Vortex Dominated Flow Fields,” AIAA 96-2499, June 1996.
7. Raj, P., Kinard, T.A. and Vermeersch, S.A., “Vortical Flow Simulation Using an Unstructured-Grid Euler Method,” ICAS-96-1.4.5, September 1996.
8. Jordan, K.J., “Euler Technology Assessment – SPLITFLOW Code Applications for Stability and Control Analysis on an Advanced Fighter Model Employing Innovative Control Concepts,” NASA CR-1998-206943, March 1998.
9. Charlton, E.F., “Numerical Stability & Control Analysis Towards Falling-Leaf Prediction Capabilities of SPLITFLOW for Two Generic High-Performance Aircraft Models,” NASA CR-1998-208730, September 1998.
10. Hoeijmakers, H.W.M., “Modeling and Numerical Simulation of Vortex Flow in Aerodynamics,” Chapter 1, AGARD-CP-494, July 1991.
11. Raj, P., “Recent Developments in the Computational Solutions of Euler Equations (Invited Paper),” Third International Congress of Fluid Mechanics, Cairo, Egypt, January 1990.
12. Thomas, J. L., Taylor, S. L., and Anderson, W. K., “Navier-Stokes Computations of Vortical Flows Over Low Aspect Ratio Wings,” AIAA-87-0207, January 1987.
13. Frink, N.T., Pirzadeh, S., and Parikh, P., “An Unstructured-Grid Software System for Solving Complex Aerodynamic Problems,” NASA CP-3291, 1995, pp. 289-308.
14. Karman, Jr., S.L., “SPLITFLOW: A 3D Unstructured Cartesian/Prismatic Grid CFD Code for Complex Geometries,” AIAA 95-0343, January 1995.
15. Raj, P., Olling, C.R., Sikora, J.S., Keen, J.M., Singer, S.W., and Brennan, J.M., “Three-dimensional Euler/Navier-Stokes Aerodynamic Method (TEAM),” WRDC-TR-87-3074 (Revised), Volumes I-III, June 1989.
16. Buening, P.G., Chan, W.M., Renze, K.J., Sondak, D.L., Chiu, I.T., and Slotnik, J.P., “OVERFLOW User’s Manual, Version 1.6ab,” NASA Ames Research Center, January 1993.
17. Michal, T.R. and Johnson, J., “A Hybrid Structured/Unstructured Grid Multi-block Flow Solver for Distributed Prallel Processing,” AIAA 97-1895, June 1997.
18. Treiber, D. A. and Muilenberg, D. A., “Euler Technology Assessment for Preliminary Aircraft Design Employing OVERFLOW Code With Multiblock Structured-Grid Method,” NASA CR-4651, March 1995.
19. Michal, T. R., “Euler Technology Assessment for Preliminary Aircraft Design - Unstructured/Structured Grid NASTD Application for Aerodynamic Analysis of an Advanced Fighter/Tailless Configuration,” NASA/CR-1998-206947, March 1998.
20. Parikh, P., Pirzadeh, S., and Loehner, R., “A Package for 3-D Unstructured Grid Generation, Finite-Element Flow Solution and Flow Field Visualization,” NASA CR-182090, 1990.

Paper: 47
Author: Dr. Raj

Question by Mr. Mendenhall: Regarding ICE model results at $\alpha = 18°$, how do you evaluate predicted results from CFD if you have no wind tunnel data to guide you during conceptual design? With no data, you might think the higher α result is the one in error.

Answer: Proper monitoring of the solution process for convergence, and interpretation of results, are critical. For $\alpha = 18°$ case, the solution actually did not reach a steady state, and pitching moment fluctuated around a mean value by as much as ± 0.03. In contrast, the higher α result was a converged solution with fluctuations of the order of ± 0.0005 about the mean value.

This page has been deliberately left blank

Page intentionnellement blanche